Mean-field kinetic theory approach to evaporation of a binary liquid into vacuum

A. Frezzotti,[1,*] L. Gibelli,[2,†] D. A. Lockerby,[2,‡] and J. E. Sprittles[3,§]
[1]*Dipartimento di Scienze e Tecnologie Aerospaziali, Politecnico di Milano, 20156 Milano, Italy*
[2]*School of Engineering, University of Warwick, Coventry CV4 7AL, United Kingdom*
[3]*Mathematics Institute, University of Warwick, Coventry CV4 7AL, United Kingdom*

(Received 20 January 2018; published 14 May 2018)

Evaporation of a binary liquid into near-vacuum conditions has been studied using numerical solutions of a system of two coupled Enskog-Vlasov equations. Liquid-vapor coexistence curves have been mapped out for different liquid compositions. The evaporation process has been investigated at a range of liquid temperatures sufficiently lower than the critical one for the vapor not to significantly deviate from the ideal behavior. It is found that the shape of the distribution functions of evaporating atoms is well approximated by an anisotropic Maxwellian distribution with different characteristic temperatures for velocity components normal and parallel to the liquid-vapor interface. The anisotropy reduces as the evaporation temperature decreases. Evaporation coefficients are computed based on the separation temperature and the maximum concentration of the less volatile component close to the liquid-vapor interface. This choice leads to values which are almost constant in the simulation conditions.

DOI: 10.1103/PhysRevFluids.3.054001

I. INTRODUCTION

The liquid-vapor phase change is a complex, multiscale process which involves length scales spanning many orders of magnitude. When the characteristic spatial scale has a macroscopic size, the liquid and vapor bulk phases are well described by hydrodynamic equations. In contrast, the structure of the liquid-vapor interfacial region is more complex, with sharp gradients in flow variables bringing in to play additional physical effects which must be accounted for in order to connect the two hydrodynamic domains. More specifically, the region separating the liquid and vapor phases comprises two subregions, namely the liquid-vapor interface itself whose size is of the order of the particles' molecular diameter [1] and, in nonequilibrium conditions, a Knudsen layer which extends a few mean free paths into the vapor side [2]. Macroscopic quantities undergo strong variations across these subregions which manifest as "jumps" at the macroscopic scale.

The standard kinetic theory literature on evaporation and condensation processes focuses on the vapor dynamics next to the liquid-vapor interface and takes into account the molecular exchanges with the liquid phase through phenomenological boundary conditions. The main aim is to resolve

*aldo.frezzotti@polimi.it
†Corresponding author: l.gibelli@warwick.ac.uk
‡d.lockerby@warwick.ac.uk
§j.e.sprittles@warwick.ac.uk

the structure of the Knudsen layer and to quantify the jumps of macroscopic flow properties across this region.

Most of the kinetic theory studies are devoted to simple gases [2,3] while very few deal with mixtures. Still, fluid flows involving phase change of multicomponent liquids are met in the study of several phenomena of both theoretical interest and practical relevance. Examples include the formation of cometary atmospheres [4], the laser-induced vaporization of solids [5], distillation processes in high vacuum conditions [6], and the modeling of biodiesel and diesel fuel droplet heating and evaporation [7].

The first kinetic theory studies which focus on the evaporation and condensation of mixtures have been based on the generalization of the moment methods that provide good results when applied to a simple gas [8,9]. However, it has been shown that the ansatz commonly used in this case fails with mixtures when the molecular weights of the components are significantly different [10].

Jump formulas for temperature, density, and mixture composition have thus been obtained in numerical form, as a function of the downstream Mach number, by solving the Boltzmann equation for a binary mixture through the direct simulation Monte Carlo (DSMC) method with hard-sphere and variable hard-sphere potentials [10]. The DSMC method has also been used to investigate the flow of a mixture of complex organic molecules between an evaporating and a condensing surface and good agreement has been found between the computed evaporation rates and experimental data [11].

A systematic investigation of the weak evaporation and condensation of a binary mixture has been carried out based on the finite-difference numerical solution of the linearized Boltzmann equation [12] and general expressions to match kinetic layers with Navier-Stokes equations have been obtained by means of the asymptotic analysis of the nonlinear Boltzmann equation [13].

The evaporation and/or condensation of a mixture has also been studied for vapor flows in a volume occupied by a different and noncondensable species for both a monatomic gas [14,15] and a binary mixture of polyatomic gases [16]. It is interesting to note that the importance of this case also extends to modeling gas flow induced by gas absorption at the walls of vacuum devices [17].

In spite of the considerable amount of research effort, many aspects of evaporation and condensation flows are still unclear. Among them, the assessment of the boundary conditions commonly adopted at the liquid-vapor interface has certainly the prominent role [18]. The need for a deeper understanding of the complexities of interfacial phenomena has triggered a number of studies based on molecular dynamics (MD) simulations of Lennard-Jones single-component [19–22] and, more recently, multicomponent fluids [23,24]. In contrast to studies based on the Boltzmann equation, MD simulations are able to model both the liquid and vapor phases within the same framework, although the high computational cost hinders their extensive use in systematic investigations.

The present paper studies the evaporation of a binary liquid into near vacuum conditions by means of a system of two coupled Enskog-Vlasov equations for a mixture of spherical atoms interacting through Sutherland potentials. Evaporation into near vacuum occurs when the backscattered molecular flux from the vapor to the liquid can be neglected. Therefore, by elucidating the statistical features of atoms spontaneously emitted by the liquid bulk, this process permits one to assess, in the simplest possible setting, kinetic boundary conditions at the liquid-vapor interface. In spite of the simplified treatment of pair correlations in the dense phase, the modeling approach used in the present study provides a realistic description of the evaporation process while keeping the computing effort at a low level compared with MD simulations. Indeed, in one-dimensional flows, the numerical solution of the proposed kinetic model is about two orders of magnitude faster than MD [25].

The rest of the paper is organized as follows:

Section II outlines the standard kinetic theory approach to evaporation and condensation processes and briefly discusses the problem related to the assessment of the boundary conditions commonly adopted at the liquid-vapor interface.

Section III contains the mathematical formulation of multicomponent fluids based on the system of coupled Enskog-Vlasov equations and a brief description of the setup of the numerical computations.

Section IV is devoted to the study of nonuniform equilibrium solutions of a binary mixture composed of two monatomic components. These solutions provide the liquid-vapor coexistence

diagram and, in particular, the saturated vapor densities as a function of the system temperature and concentration. These quantities play a fundamental role in the calculation of the evaporation coefficients. Furthermore, equilibrium density profiles are used to validate the numerical code.

Section V focuses on the near vacuum evaporation of an equimolar binary mixture composed of two monatomic components. The aim of the investigation is twofold: first, to obtain the distribution functions of atoms initially in the liquid phase and entering the vapor region, and second, to provide an estimate of the evaporation coefficients as a function of reference temperature and composition of the liquid-vapor interface.

Section VI summarizes and comments on the main findings of the paper.

II. STANDARD KINETIC THEORY APPROACH

The common basis of fundamental kinetic theory studies on evaporation and condensation processes for a mixture of N components is a system of coupled, steady, and spatially one-dimensional Boltzmann equations of the form

$$v_z \frac{\partial f_i}{\partial z} = \sum_{j=1}^{N} \mathcal{C}_{ij}(f_i, f_j), \quad i = 1, \ldots, N, \tag{1}$$

where the single spatial coordinate z spans the direction normal to the liquid-vapor interface, $f_i(z,\mathbf{v})$ is the distribution function of molecular velocities $\mathbf{v}$ of the i component at the spatial location z, and $\mathcal{C}_{ij}(f_i, f_j)$ is the collision integral representing the interaction between components i and j.

It is worth noticing that the assumption that the evaporation is a steady and one-dimensional process is not a serious limitation. Indeed, jump relationships derived in such conditions can also be used in unsteady flows and/or when the liquid-vapor interface is not planar as long as hydrodynamic regions evolve slowly on the timescale of the mean free time and the Knudsen layer thickness is small when compared with the curvature of the liquid-vapor interface [26].

The bulk of the liquid phase is commonly assigned fixed properties and the detailed physical structure of the liquid-vapor interface is strongly simplified by reducing it to a surface bounding the vapor. Molecular exchanges through this surface are modeled by inhomogeneous linear boundary conditions for the distribution functions. More specifically, in the simplest case of evaporation into near vacuum conditions, the following boundary conditions are assumed to hold at the evaporating surface:

$$f_i(z = 0, \mathbf{v}) = \alpha_{e,i} n_i^{(eq)} \left(\frac{m_i}{2\pi k T_l} \right)^{3/2} \exp\left(-\frac{m_i \mathbf{v}^2}{2 k T_l} \right), \tag{2}$$

where k is the Boltzmann constant, T_l is the temperature of the liquid-vapor interface, and m_i, $n_i^{(eq)}$,$\alpha_{e,i}$ are the mass, the saturated vapor density, and the evaporation coefficient of the i component, respectively. In most of the cases, a unit evaporation coefficient is assumed for all the components and both the temperature of the liquid-vapor interface and the saturated vapor densities are kept constant.

Several experimental studies have been carried out over the years in an attempt to assess the kinetic boundary conditions at the liquid-vapor interface. In contrast to the boundary condition (2), recent experiments on the evaporation of helium dissolved in hydrocarbon liquids have shown that evaporated atoms exhibit a slightly higher kinetic energy distribution compared to the Maxwellian at the temperature of the liquid surface [27]. On the other hand, the measurements of the evaporation and condensation coefficients are inconclusive, covering a remarkable three orders of magnitude [28,29].

In the case of a single-component fluid, the kinetic boundary conditions have also been investigated based on MD simulations [19,20,30] and mean-field approximations of simple liquids [31,32]. The results show that the half-range Maxwellian provides a good approximation of the distribution function of the evaporating atoms in the case of near-vacuum evaporation while deviations have

been reported in the presence of a significant molecular flux impinging on the liquid surface [20]. Very few studies have been carried out for a multicomponent liquid [23,24], mainly due to the computational effort required for a detailed investigation of the problem. It is thus unclear whether or not the results obtained for the single-component case can be extended to mixtures.

It is worth noting that, in general, the evaporation rates of different species of a multicomponent liquid are not the same. Therefore, the saturated vapor densities of the component, $n_i^{(eq)}$ in Eq. (2), should vary in time unless it is assumed that some artificial mechanism keeps the surface composition constant. Actually, in some cases, the assumption of constant interface composition is not unreasonable since the change of the surface composition might be slow in comparison with the fast characteristic kinetic timescale in the vapor. However, a more realistic treatment of the evaporation of a multicomponent liquid certainly requires one to couple vapor and liquid phases [29].

The proposed approach based on the Enskog-Vlasov equations is well suited to assessing the boundary conditions commonly used by kinetic theory studies at the liquid-vapor interface, since it is for less computationally demanding than MD simulations while having the natural capability of handling both the liquid and vapor phases, including the interface region.

III. MEAN-FIELD KINETIC THEORY APPROACH

A. The Enskog-Vlasov equation

An approximate kinetic theory modeling of simple and multicomponent fluids exhibiting phase separation has been studied by several authors [31,33–35] and applied to investigate a wide range of two-phase flows. Examples include condensation and evaporation processes [31,32,36], gas-surface interactions [37,38], adsorbed gas layers [39], and formation and breakage of liquid menisci [40].

Following these references, let us consider a mixture composed of spherical particles having masses m_i and diameters σ_i, with $i = 1, \ldots, N$ being N the number of components. The particles are supposed to interact through the Sutherland potentials, ψ_{ij}, which are obtained by superimposing soft attractive tails, enabling the existence of a condensed phase, to the hard sphere repulsive potentials, that is,

$$\psi_{ij}(r) = \begin{cases} +\infty, & r \leqslant \sigma_{ij} \\ -\phi_{ij}\left(\frac{\sigma_{ij}}{r}\right)^{\gamma_{ij}}, & r > \sigma_{ij} \end{cases}, \tag{3}$$

where $r = \|\mathbf{r}_* - \mathbf{r}\|$ is the distance between the interacting particles located at $\mathbf{r}$ and $\mathbf{r}_*$, $\sigma_{ij} = (\sigma_i + \sigma_j)/2$, whereas ϕ_{ij} and γ_{ij} are positive constants which are related to the depth of the potential wells at $r = \sigma_{ij}$ and to the range of the soft interactions between the species i and j, respectively. Note that the algebraic form of the potential tails in Eq. (3) is not mandatory and more general expression can be used.

The adoption of simplifying assumptions about pair correlations allows the derivation of the following kinetic equations for the one-particle distribution functions $f_i(\mathbf{r},\mathbf{v},t)$ of fluid atoms:

$$\frac{\partial f_i}{\partial t} + \mathbf{v}\cdot\nabla_{\mathbf{r}} f_i + \frac{\boldsymbol{\mathcal{F}}_i[\mathbf{n}]}{m_i}\cdot\nabla_{\mathbf{v}} f_i = \mathcal{C}_i[\mathbf{f}], \quad i = 1, \ldots, N, \tag{4a}$$

where square brackets denote the functional dependence on the whole set of distribution functions and density fields, $\boldsymbol{f} = \{f_i\}$ and $\boldsymbol{n} = \{n_i\}$, respectively. In Eq. (4a), the self-consistent force fields generated by the potential tails, $\boldsymbol{\mathcal{F}}_i$, and the hard-sphere collision integrals, $\mathcal{C}_i$, are given by the following expressions:

$$\boldsymbol{\mathcal{F}}_i[\mathbf{n}] = \sum_{j=1}^{N} \int_{r>\sigma_{ij}} \frac{d\psi_{ij}}{dr} \frac{\mathbf{r}_* - \mathbf{r}}{\|\mathbf{r}_* - \mathbf{r}\|} n_j(\mathbf{r}_*, t)\, d\mathbf{r}_*, \tag{4b}$$

$$\mathcal{C}_i[\mathbf{f}] = \sum_{j=1}^{N} \sigma_{ij}^2 \int_{\mathcal{R}^3} \int_{\mathcal{S}_+} \{\chi_{ij}[\mathbf{n}](\mathbf{r}, \mathbf{r} + \sigma_{ij}\tilde{\mathbf{k}}) f_i(\mathbf{r} + \sigma_{ij}\tilde{\mathbf{k}}, \mathbf{v}_*', t) f_j(\mathbf{r}, \mathbf{v}', t)$$

$$- \chi_{ij}[\mathbf{n}](\mathbf{r}, \mathbf{r} - \sigma_{ij}\tilde{\mathbf{k}}) f_i(\mathbf{r} - \sigma_{ij}\tilde{\mathbf{k}}, \mathbf{v}_*, t) f_j(\mathbf{r}, \mathbf{v}, t)\} (\mathbf{v}_r \cdot \tilde{\mathbf{k}}) d\mathbf{v}_* d^2\tilde{\mathbf{k}}, \tag{4c}$$

where χ_{ij} are the contact values of the pair correlation functions of hard-sphere fluids in equilibrium and the precollisional velocities $\mathbf{v}'$ and $\mathbf{v}_*'$ are changed into $\mathbf{v}$ and $\mathbf{v}_*$ according to the dynamics of binary encounters. The latter depends on the relative velocity $\mathbf{v}_r = \mathbf{v}_* - \mathbf{v}$ of two colliding atoms and on the orientation of the unit impact vector $\tilde{\mathbf{k}}$ with respect to $\mathbf{v}_r$, that is,

$$\mathbf{v}' = \mathbf{v} + (\mathbf{v}_r \cdot \tilde{\mathbf{k}})\tilde{\mathbf{k}}, \tag{4d}$$

$$\mathbf{v}_*' = \mathbf{v}_* - (\mathbf{v}_r \cdot \tilde{\mathbf{k}})\tilde{\mathbf{k}}. \tag{4e}$$

Equations (4), which are referred to as Enskog-Vlasov kinetic equations, describe a hard sphere multicomponent fluid under the action of the self-consistent force fields generated by the soft attractive tails.

For the sake of simplicity, in the following it is supposed that atoms of different species have the same diameter, $\sigma_i = \sigma$, for all i. Accordingly, the pair correlation functions of different species simplify to the one valid for the single-component case [41] and subscripts can be omitted. Notice should be made that expressions of pair correlation functions have also been derived for mixture of hard spheres having a different diameter and, therefore, the present study can be extended to deal with this case as well [42].

In the standard Enskog theory (SET), χ is approximated by using the value of the pair correlation function in a fluid in *uniform equilibrium* with density $n(\mathbf{r} + \sigma/2\tilde{\mathbf{k}})$. An approximate but accurate expression for χ_{SET} can be obtained from the equation of state of the hard sphere fluid proposed by Carnahan and Starling [43] as

$$\chi_{\mathrm{SET}}(n) = \frac{1}{nb}\left(\frac{p^{hs}}{nkT} - 1\right) = \frac{1}{2}\frac{2-\eta}{(1-\eta)^3}, \qquad b = \frac{2\pi\sigma^3}{3}, \quad \eta = \frac{\pi\sigma^3 n}{6}. \tag{5}$$

Theoretical properties of SET have been considerably improved in revised Enskog theory (RET) [44], where χ_{RET} is the contact value of the pair correlation function in a fluid in *nonuniform equilibrium*. The use of RET formulation is more difficult since the pair correlation function is a functional of the density field. Although an expression can be obtained as a formal cluster expansion in the density, in practical applications simpler approximations are recommended. Following Ref. [45], in the present work the pair correlation function at contact has been computed from the simpler χ_{SET} by replacing the actual value of the density at the contact point of two colliding spheres with the value of the density field averaged over a spherical volume of radius σ, namely,

$$\chi[n](\mathbf{r}, \mathbf{r} - \sigma\tilde{\mathbf{k}}) = \chi_{\mathrm{SET}}\left[\overline{n}\left(\mathbf{r} - \frac{\sigma}{2}\tilde{\mathbf{k}}\right)\right], \tag{6}$$

where

$$\overline{n}(\mathbf{r}, t) = \frac{3}{4\pi\sigma^3}\int_{\mathbb{R}^3} n(\mathbf{r}_*, t) w(\mathbf{r}, \mathbf{r}_*)\, d\mathbf{r}_*, \quad w(\mathbf{r}, \mathbf{r}_*) = \begin{cases} 1, & \|\mathbf{r}_* - \mathbf{r}\| < \sigma \\ 0, & \|\mathbf{r}_* - \mathbf{r}\| > \sigma \end{cases}. \tag{7}$$

Similar approximations are used in density functional theories of nonuniform fluids and considerably improve the results of SET [46].

B. Simulation method

It may be assumed that, below the critical temperature, the liquid and vapor occupy regions separated by a planar interface. Therefore, in the following, a spatially one-dimensional form of

the kinetic model (4) is considered. Furthermore, a binary mixture is studied which is assumed to be composed of atoms having the same diameter σ interacting through the following Sutherland potentials:

$$\psi_{aa}(r) = \begin{cases} +\infty, & r < \sigma \\ -\phi_{aa}\left(\frac{\sigma}{r}\right)^{\gamma}, & r \geqslant \sigma \end{cases}, \tag{8a}$$

$$\psi_{bb}(r) = \begin{cases} +\infty, & r < \sigma \\ -\phi_{bb}\left(\frac{\sigma}{r}\right)^{\gamma}, & r \geqslant \sigma \end{cases}, \tag{8b}$$

$$\psi_{ab}(r) = \psi_{ba}(r) = \begin{cases} +\infty, & r < \sigma \\ -\phi_{ab}\left(\frac{\sigma}{r}\right)^{\gamma}, & r \geqslant \sigma \end{cases}. \tag{8c}$$

The numerical solution of the system of two coupled Enskog-Vlasov equations is achieved by an extension of the classical DSMC particle scheme to dense fluids [47]. According to this approach, the distribution functions of the different species are represented by computational particles whose positions and velocities evolve in time by a sequence of time steps, each of them consisting of a free flight and a local collision substeps. The former corresponds to the streaming operator at the left-hand side of Eq. (4a), while the latter is performed according to stochastic rules, consistent with the structure of the collision terms given by Eq. (4c). Macroscopic fluid properties are obtained by averaging particles' microscopic states.

Unless otherwise stated, we have set $m_b/m_a = 1, \gamma = 6$, and $\phi_{aa}/(kT_0) = 1, \phi_{bb}/(kT_0) = 0.75, \phi_{ab}/(kT_0) = 1.25$, with T_0 being a reference temperature. The value adopted for the soft potential exponent permits to have the same asymptotic behavior of a 12-6 Lennard-Jones potential [48] while the depths of the potential wells have been chosen so as to simulate a nonsymmetrical binary mixture composed of species with different volatility. Note that ϕ_{ab} is significantly larger than the value prescribed by the usual Lorentz-Berthelot combining rule which, in most of the cases, overestimates the well depth of the unlike interaction in mixtures composed of simple molecules [49]. However, this choice strongly couples the evaporation of each component, allowing the study of simultaneous evaporation of each species (as opposed to a sequential evaporation). The successive evaporation of two pure liquids is clearly shown by MD simulations in Ref. [50] where the pressure jump evaporation of a nanodroplet composed of a mixture of Lennard-Jones molecules is studied by setting ϕ_b/ϕ_a similar to the present study and ϕ_{ab} as given by Lorentz-Berthelot combining rule.

The number of computational particles has been set to 10^6 and, as customary in one- and two-dimensional DSMC simulations, it is made equal to the number of real atoms by a proper choice of the cross section of the computational domain normal to the nonhomogeneous direction z. The computational domain has been divided into a number of cells with size $1/20\,\sigma$ and the time step has been set equal to $5 \times 10^{-4}\, m_a^{1/2}/(kT_0)^{1/2}\sigma$.

IV. EQUILIBRIUM SIMULATIONS: PHASE COEXISTENCE DIAGRAM

There are two main reasons to determine the liquid-vapor coexistence diagram before studying evaporation into vacuum. First, it provides the saturated vapor densities as a function of the system temperature. These quantities are needed to evaluate the evaporation coefficients [see Eq. (12)]. Second, the liquid-vapor coexistence diagram can be used to provide a validation of the numerical code used to simulate the evaporation of a binary liquid into near vacuum conditions.

The phase coexistence diagram of multicomponent liquid is mapped out by using two different approaches. The first approach consists in requiring that the system is in thermal, mechanical, and chemical equilibrium, namely with constant temperature, pressure, and chemical potential across the two phases. This amounts to solving the following system of three nonlinear algebraic equations in the five unknowns given by the densities, $n^{(v)}, n^{(l)}$; the molar fractions of the a component, $c^{(v)}, c^{(l)}$,

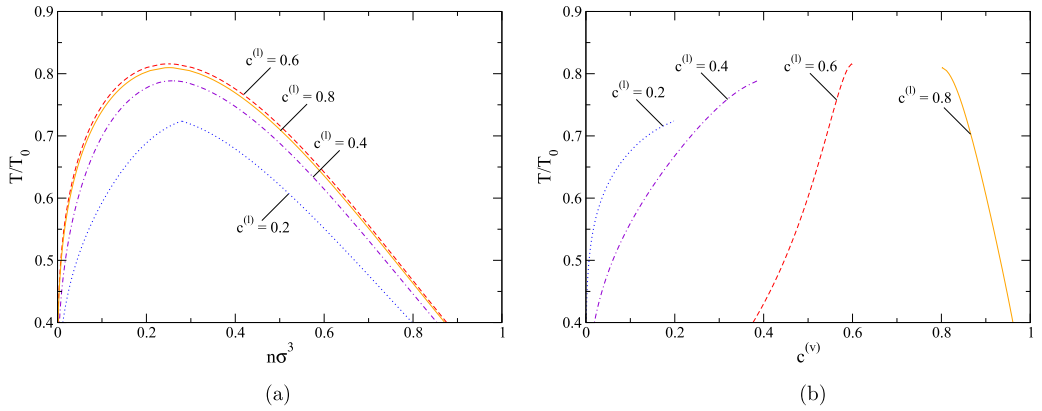

FIG. 1. Equilibrium simulations. Phase diagram of the binary mixture for different molar fractions of the a component in the liquid phase. (a) Temperature vs density. (b) Temperature vs vapor molar fraction.

of the coexisting vapor and liquid phases; and the temperature T of the system:

$$p(n^{(v)},c^{(v)},T) = p(n^{(l)},c^{(l)},T), \tag{9a}$$

$$\mu_a(n^{(v)},c^{(v)},T) = \mu_a(n^{(l)},c^{(l)},T), \tag{9b}$$

$$\mu_b(n^{(v)},c^{(v)},T) = \mu_b(n^{(l)},c^{(l)},T). \tag{9c}$$

In practice, the system of Eq. (9) is solved for various prescribed values of the temperature and molar fraction of the a component in the liquid phase.

The chemical potentials, $\mu_{a,b}$, and the pressure, p, of a binary mixture whose components interact through the Sutherland potentials given by Eqs. (8) have two contributions. One comes from the hard-sphere repulsive potential [51] and one from the soft-attractive potential tail [52]. The overall expression reads

$$\mu_a = kT\left[\eta\frac{8-9\eta+3\eta^2}{(1-\eta)^3}+\ln(c\eta)\right]-8\eta\frac{\gamma}{\gamma-3}[c\phi_{aa}+(1-c)\phi_{ab}], \tag{10a}$$

$$\mu_b = kT\left\{\eta\frac{8-9\eta+3\eta^2}{(1-\eta)^3}+\ln[(1-c)\eta]\right\}-8\eta\frac{\gamma}{\gamma-3}[c\phi_{ab}+(1-c)\phi_{bb}], \tag{10b}$$

$$p = \frac{6}{\pi}\eta\frac{1+\eta+\eta^2-\eta^3}{(1-\eta)^3}kT-\frac{24}{\pi\sigma^3}\eta^2\frac{\gamma}{\gamma-3}[c^2\phi_{aa}+2c(1-c)\phi_{ab}+(1-c)^2\phi_{bb}]. \tag{10c}$$

The phase diagram is displayed in Fig. 1. More specifically, Fig. 1(a) shows the temperature versus the density while Fig. 1(b) shows the temperature versus the molar fraction of a component in the vapor phase.

The phase diagram can also be mapped out based on the equilibrium density profiles obtained from long-time numerical solutions of the system of two coupled Enskog-Vlasov equations. The spatial domain is a finite symmetric interval $[60\,\sigma,60\,\sigma]$ of the z axis and periodic boundary conditions have been assumed at $z=\pm 60\,\sigma$. Each computation is started by arranging a homogeneous liquid slab of width $80\,\sigma$ at temperature T in the middle of the computational domain bounded by two symmetrical empty regions. The thickness of the slab is chosen much wider than the thickness of the liquid-vapor interface to be formed during the simulation.

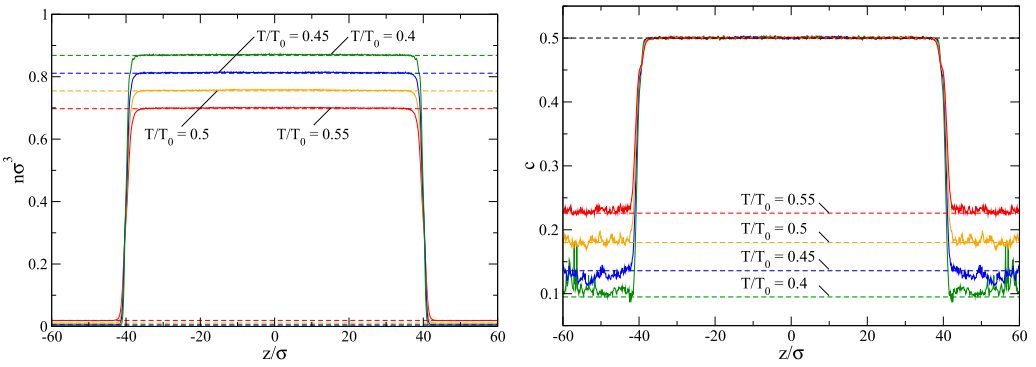

FIG. 2. Equilibrium simulations. Density and molar fraction of the a component of the mixture (which is equimolar in the liquid phase) for different temperatures. Solid lines: results provided by the numerical solution of the system of two coupled Enskog-Vlasov equations, Eqs. (4) with $N = 2$. Dashed lines: predictions based on Eqs. (9). (a) Density. (b) Molar fraction.

The evolution of the system is then computed until the evaporation of part of the liquid brings the liquid and vapor in equilibrium. In order to keep the temperature of the system constant during the transient evaporation phase, a simple Gaussian thermostat [53] is applied during the whole simulation to a central strip of liquid with width of $60\,\sigma$.

Numerical experiments have shown that the final composition of the liquid phase is slightly different from the one which is initially prescribed. Therefore, in order to enforce a constant liquid composition, the following procedure has been adopted. Every time step, in the thermostatted region, randomly selected atoms of the component in excess are replaced with atoms of the lacking component. This procedure is carried out until the initial transient that leads to the formation of the interface dies out. Thereafter, the system is allowed to evolve freely.

Figure 2 shows densities and compositions of the liquid and vapor phases for a mixture that is equimolar in the liquid phase. Dashed lines are the constant values of vapor and liquid density far from the interface as given by the liquid-vapor coexistence curve determined based on Eqs. (9), while solid lines are the results obtained by numerically solving the coupled system of Enskog-Vlasov equations. The agreement between the two approaches is good and this provides a validation of the numerical code.

V. NONEQUILIBRIUM SIMULATIONS: EVAPORATION INTO VACUUM

Nonequilibrium simulations have been carried out to study the evaporation of an equimolar binary liquid into near vacuum conditions at the temperatures $T/T_0 = [0.4, 0.45, 0.5, 0.55]$, with the critical temperature $T_c/T_0 \simeq 0.8139$. This range of temperature values has been selected as a compromise between the two contrasting needs of having a rarefied vapor and a sufficient number of atoms of both species in the vapor phase.

Table I summarizes the initial densities and concentrations of the two components in the liquid and vapor phases as well as the compressibility factor of the mixture, Z. In the lower temperature case, Z is sufficiently close to unity to safely infer that the vapor behavior is almost ideal, while at higher temperatures, slight deviations from the ideal are anticipated. It is worth noticing, however, that the compressibility factor has been computed based on the equilibrium density. Since the density of the vapor during evaporation is lower than the one in equilibrium, deviations from the ideal behavior are less than the ones suggested by Table I.

Each simulation has been started from the equilibrium solutions obtained as described in the previous section. In all cases, the liquid slab thickness is about $80\,\sigma$. This large initial slab thickness

TABLE I. Overview of the parameters which characterize the equilibrium states in dimensionless form: Temperature of the liquid, T/T_0; density of the liquid phase, $n^{(l)}\sigma^3$; density of the vapor phase, $n^{(v)}\sigma^3$; molar fraction of the a component in the liquid phase, $c^{(l)}$; molar fraction of the a-component in the vapor phase, $c^{(v)}$; and compressibility factor of the mixture, $Z = p[c^{(v)}m_a + (1-c^{(v)})m_b]/(n^{(v)}kT)$.

T/T_0	$n^{(l)}\sigma^3$	$n^{(v)}\sigma^3$	$c^{(l)}$	$c^{(v)}$	Z
0.4	0.868309	0.0020255	0.5	0.0949	0.9865
0.45	0.811173	0.0051217	0.5	0.1359	0.9697
0.5	0.754604	0.0106136	0.5	0.1801	0.9422
0.55	0.697613	0.0192752	0.5	0.2260	0.9038

is necessary to run sufficiently long simulations and collect enough atoms in the vapor phase to compute the quantities of interest. Periodic boundary conditions along the z direction have been replaced with absorbing surfaces that remove from the simulation box those atoms whose distance from the receding liquid-vapor interface exceeds a specified threshold; this has been set to $10\,\sigma$. This distance is large enough not to influence the interface structure, but, at the same time, it is small in comparison with the vapor mean free path.

The desired temperature level has been obtained by applying a Berendsen thermostat in a central strip of the liquid slab of initial width $40\,\sigma$. Compared to the Gaussian, the Berendsen thermostat allows for temperature fluctuation and is expected to be more suitable to nonequilibrium simulations since it provides a good compromise between disturbing the physical behavior of the system and maintaining possibly gradients of temperature, pressure and so on [54]. However, numerical experiments have shown that results are not significantly affected by this choice. The strip thickness has been gradually reduced in time following the interface motion.

Macroscopic quantities have been obtained using a sampling time of $40\,t_0$, where $t_0 = m_a^{1/2}/(kT_0)^{1/2}\sigma$ is the characteristic dimensionless time, the number of samples being 100.

In order to reduce the statistical noise, results from four independent simulations of the same flow field have been superposed.

A. Macroscopic quantities

Mixture density, composition, and longitudinal velocity snapshots at dimensionless times $t/t_0 = (1,2,3,4) \times 10^3$ are shown in Fig. 3(a).

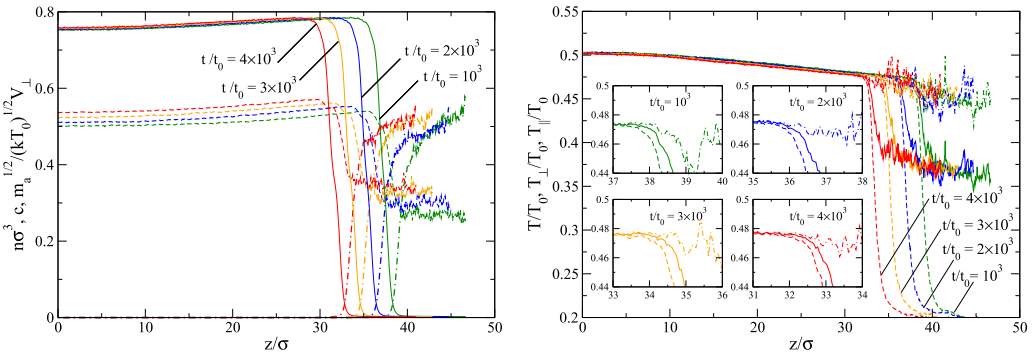

FIG. 3. Nonequilibrium simulations. Macroscopic quantities at different times for $T/T_0 = 0.5$. (a) Density (solid), concentration (dashed), and longitudinal velocity (dashed-dotted). (b) Full (solid), longitudinal (dashed), and transversal (dash-dotted) temperatures.

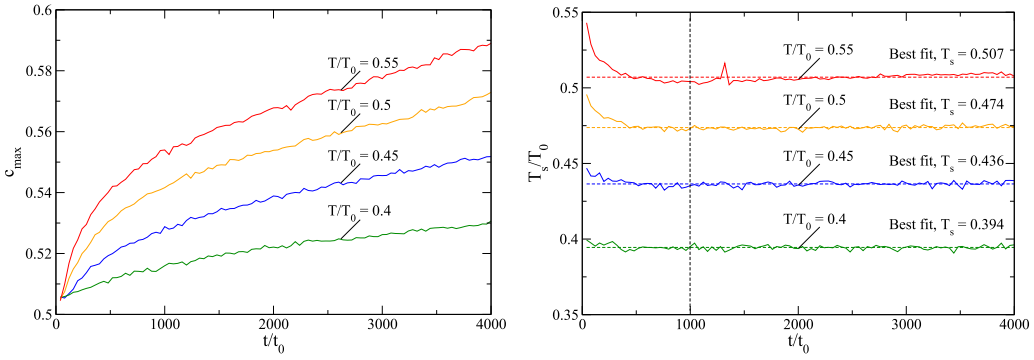

FIG. 4. Nonequilibrium simulations. Time histories of the maximum molar fraction of the less volatile a component and the separation temperature for different temperatures. (a) Maximum concentration. (b) Separation temperature.

During evaporation, the total density profile recedes while maintaining on almost constant shape. However, the preferential evaporation of the most volatile b component causes a continuous change of the system composition both in the liquid and in the vapor phase, which leads to the surface becoming richer in the a component. Accordingly, the concentration of the mixture, defined as the molar fraction of the a component, has a maximum which, as shown in Fig. 4(a), increases monotonically in time.

Figure 3(b) reports the full temperature along with the longitudinal and transversal temperatures. The latter measure the dispersion of the full distribution function along the directions perpendicular and parallel to the liquid-vapor interface. As expected, within the liquid bulk, the longitudinal and transversal temperatures superimpose with the value of the full temperature which, outside the thermostatted strip, shows a linearly decreasing profile due to the evaporative cooling. Temperatures separate in the proximity of the interface center, with the longitudinal one, which exhibits the strongest drop in the outermost region of the interface, reaching a minimum in the vapor region. The location where the temperatures separate marks the beginning of a transition layer which extends a few molecular diameters into the low-density vapor region and in which the atoms' dynamics is primarily affected by the mean force field. The temperature evaluated at that location is referred to as separation temperature, T_s, and, as discussed in the following subsection, its value contributes to define the velocity distribution functions of evaporating atoms. It worth stressing that, after the initial transient, the separation temperature keeps a constant value, as clearly shown in Fig. 4(b).

B. Velocity distribution functions

As noted in previous investigations [19–21,31], the backscattered vapor component is virtually absent in simulating evaporation in near-vacuum conditions. Therefore, it is possible to obtain the shape of the distribution function of atoms spontaneously emitted by the liquid bulk simply by recording events of atoms crossing a sufficiently close control surface located in the vapor region. In the present study, this distance has been set to $10\,\sigma$ from the interface, whose position is defined by the maximum slope of the total density profile.

Figure 5 shows the normalized reduced distribution functions of velocity components normal and parallel to the liquid-vapor interface are well approximated by Maxwellians, as found for a single-component fluid in similar conditions [19–21,31]. However, as the temperature of the system increases, the difference between the parameters that enter as normal and parallel temperatures in the half-range Maxwellians, $\theta_\perp$ and $\theta_\parallel$, respectively, becomes larger. Note that these parameters cannot be identified with the longitudinal and transversal temperatures discussed in the previous section since

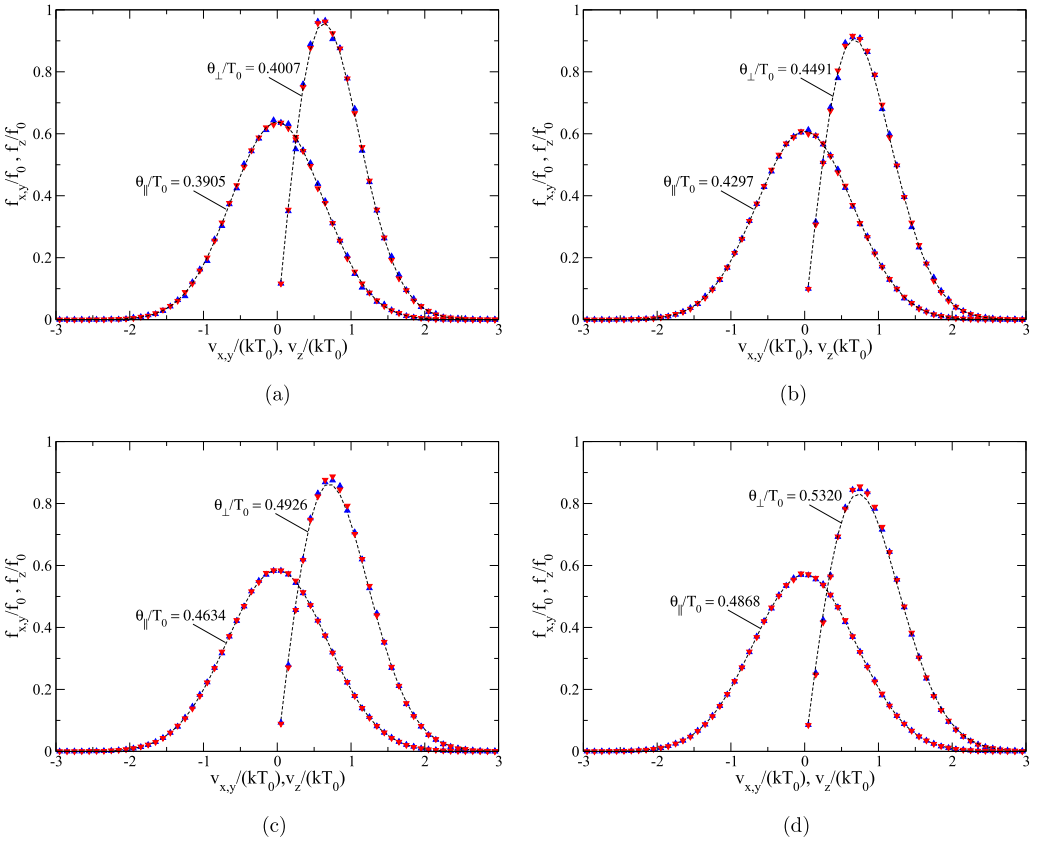

FIG. 5. Nonequilibrium simulations. Reduced normalized distribution functions of the evaporated atoms. Solid blue triangles up and solid red triangles down are the numerical results for the a component and b component, respectively. Dashed black lines are the best Maxwellian fits. Temperatures of the latter are explicitly reported and the percentage errors do not exceed 1%. (a) $T/T_0 = 0.4$. (b) $T/T_0 = 0.45$. (c) $T/T_0 = 0.5$. (d) $T/T_0 = 0.55$.

the Maxwellians reported in Fig. 5 are defined only for $v_z > 0$, while $T_\perp$ and $T_\parallel$ are moments of the full-range distribution function. The anisotropy of the distribution function of atoms evaporating into near vacuum has already been found by previous molecular dynamics (MD) simulations and it was attributed to the hard-sphere collisions in the liquid-vapor interface, which become more important as the temperature of the system increases [20,55]. Interestingly, as can be easily inferred from Table II,

TABLE II. Nonequilibrium simulations. Separation temperature, T_s/T_0, temperatures of the Maxwellian distribution functions based on velocity components normal and parallel to the liquid-vapor interface, $\theta_\perp/T_0$ and $\theta_\parallel/T_0$, and their relative difference for different temperatures of the system, T/T_0.

T/T_0	T_s/T_0	$\theta_\perp/T_0$	$\theta_\parallel/T_0$	$(\theta_\perp - \theta_\parallel)/T_0$
0.40	0.394	0.4007	0.3905	0.02548
0.45	0.436	0.4491	0.4297	0.04311
0.50	0.474	0.4926	0.4634	0.05840
0.55	0.507	0.5320	0.4868	0.08218

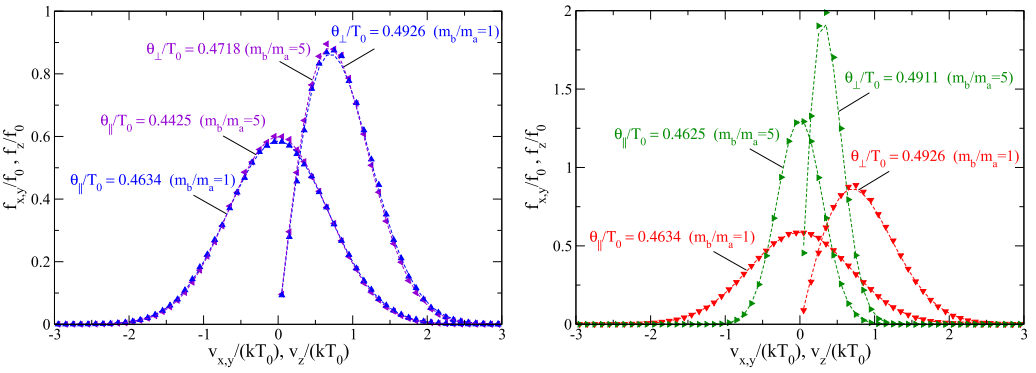

FIG. 6. Nonequilibrium simulations. Reduced normalized distribution functions of the evaporated atoms for different mass component ratios. Solid blue triangles up and solid red triangles down are the numerical results for the a component and b component, respectively, for $m_b/m_a = 1$. Solid violet triangles left and solid green triangles right are the numerical results for the a component and b component, respectively, for $m_b/m_a = 5$. Dashed black lines are the best Maxwellian fits. Temperatures of the latter are explicitly reported and the percentage errors do not exceed 1%. (a) a component. (b) b component.

the average value of the Maxwellians' temperatures, $(\theta_\perp + 2\theta_\parallel)/3$, is very close to the separation temperature T_s.

These results suggest that the distribution function of evaporating atoms can be approximated by an anisotropic Maxwellian. Accordingly, the boundary conditions at the evaporating surface, Eq. (2), should be modified as follows:

$$f_i(0,\mathbf{v}) = \frac{\alpha_{e,i}}{\delta^{1/2}\epsilon} n_i^{(eq)} \left(\frac{m_i}{2\pi k T_s}\right)^{3/2} \exp\left(-\frac{m_i v_z^2}{2k\delta T_s}\right) \exp\left(-\frac{m_i\left(v_x^2+v_y^2\right)}{2k\epsilon T_s}\right), \quad i = a,b, \tag{11}$$

where $(\delta + 2\epsilon)/3 = 1$. More specifically, a direct inspection of Table II yields $\delta = 1.02, 1.03, 1.04, 1.05$ and $\epsilon = 0.991, 0.985, 0.977, 0.960$ for $T/T_0 = 0.4, 0.45, 0.5, 0.55$.

Note that the simulation results reported above refer to a mixture whose components have the same mass. Figure 6 shows that the distribution function of evaporated atoms is anisotropic even when the two components have a very different mass, namely $m_2/m_1 = 5$. Even in this case, a relationship can be presumably established between the separation temperature and the temperatures of the reduced distribution functions normal and parallel to the liquid-vapor interface. It is expected that this relationship depends on the species mass ratio. However, more extensive study is needed to support this conjecture, which is beyond the scope of the present paper.

C. Evaporation coefficients

The evaporation coefficients of the two evaporating components are given by the expression

$$\alpha_{e,i} = \frac{\Phi_i}{n_i^{(eq)}(c_{\max}, T_s)\sqrt{\frac{k\delta T_s}{2\pi m_i}}}, \quad i = a,b, \tag{12}$$

where Φ_i is the evaporating flux of the i component in the free molecular regime and $n_i^{(eq)}$ is the saturated vapor density of the i component, provided by the liquid-vapor coexistence diagram for a binary liquid, with concentration equal to the maximum molar fraction of the less volatile component, $c_{\max}$, and the temperature given by the separation temperature, T_s. The denominator in Eq. (12) is

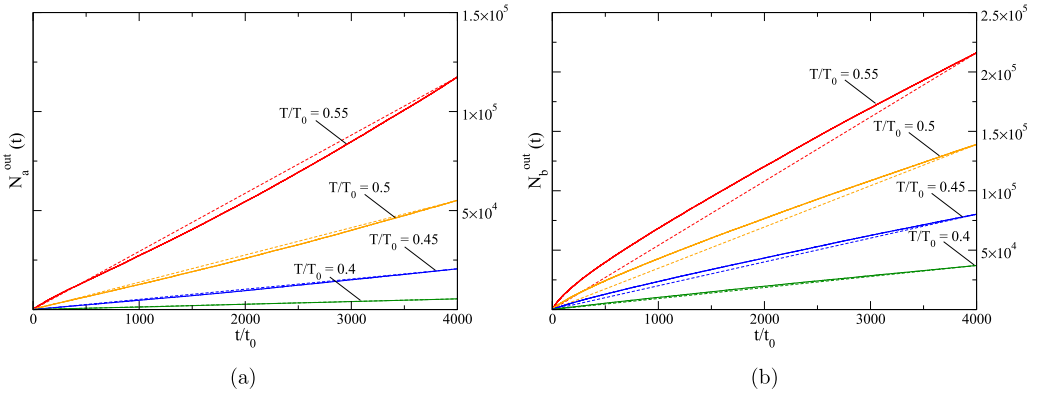

FIG. 7. Nonequilibrium simulations. Time histories of the number of evaporated atoms for the two components at different temperatures. Solid lines are the numerical results. Dashed straight lines are included to guide the eyes. (a) Less volatile a component. (b) More volatile b component.

the mass flow rate of the i component as predicted by Eq. (11) which simplifies to the classical Hertz-Knudsen equation when the anisotropy of the velocity distribution function is neglected.

It is worth stressing that the evaporation coefficients are needed to match the continuum description of the liquid phase with the kinetic theory description of the vapor phase [56]. Therefore, besides representing the local state of the interface, the concentration and temperature that enter in their definition should be predicted by a continuum model for the liquid dynamics. This is the case of $c_{\max}$ and T_s since they mark out the beginning of the liquid region whose properties could be described by hydrodynamic equations. In other words, if the interface is modeled as a surface, they are the values on the liquid side of the liquid-vapor boundary (across which jumps in parameters are expected). As a matter of fact, the locations where $c = c_{\max}$ and $T = T_s$ are different but the mismatch is of the order of few molecular diameters and it can be thus disregarded in practical applications where the temperature gradient in the liquid phase leads to negligible variations of the temperature over distances of the order of the molecular diameter.

Time histories of surface composition, $c_{\max}(t)$, and separation temperature, $T_s(t)$, are presented in Figs. 4(a) and 4(b), respectively. For each value of them, the equilibrium partial vapor densities, $n_i^{(eq)}$ in Eq. (12), have been obtained from Eqs. (9).

The fluxes $\Phi_i(t)$ have been obtained from simulations by recording the numbers of atoms of the i component removed from the domain after crossing the absorbing surfaces, $N_i(t)$. As shown in Fig. 7, the fluxes, which are defined as the first time derivatives of $N_i(t)$, are not constant because of the surface composition change. More specifically, the flux of b component decreases, whereas the flux of a component slightly increases.

The evaporation coefficients have been obtained from Eq. (12) by using the evaporating fluxes Φ_i averaged over a period of $400\,t_0$ after the initial transient has died out, i.e., $t \gtrsim 400\,t_0$. Note that during the evaporation process, the composition of the liquid-vapor interface changes in time and, accordingly, the curves shown in Fig. 8 start for $c > 0.5$ even though the two-component liquid is initially equimolar. The numerical results indicate that the evaporation coefficients are not the same for the two components and they only mildly depend on temperature and composition of the liquid-vapor interface with all in the range $[0.85, 1]$. More specifically, using the constant evaporation coefficients $\alpha_{e,a} = 0.95$ and $\alpha_{e,b} = 0.91$ leads to a percentage error on the predicted evaporation mass flow rate which is within 5%.

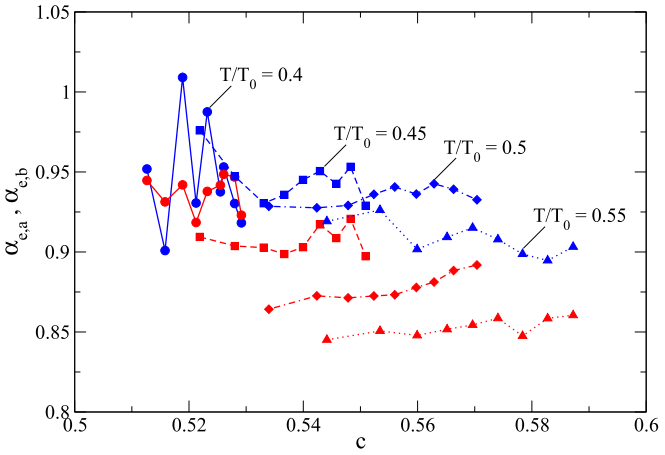

FIG. 8. Nonequilibrium simulations. Evaporation coefficients of the *a* component (blue symbols and lines) and of the *b* component (red symbols and lines) for different temperatures as a function of the interface composition. The accuracy of the results is within 5%.

VI. CONCLUSIONS

Evaporation into near vacuum conditions of a binary liquid has been investigated through a mean-field kinetic theory approach based on a system of two coupled Enskog-Vlasov equations for a mixture of spherical atoms interacting through Sutherland potentials.

In spite of the simplified description of the microscopic dynamics, the proposed modeling approach leads to a unified description of both the liquid and vapor phases and it thus permits us to critically assess the boundary conditions that are commonly assumed at the liquid-vapor interface by standard kinetic theory studies, while being far computationally cheaper than MD.

The phase diagram has been determined by using two different approaches: first, by solving the nonlinear system of algebraic equations obtained by requiring that the pressure and the chemical potentials of the two components are the same in the two phases, and second, by numerically solving the system of two coupled Enskog-Vlasov equations. In the latter case, a strip of liquid is initially placed in the middle of a domain and gas elsewhere with periodic boundary conditions. The system is then allowed to evolve until a steady state is reached and the phase diagram has been obtained by evaluating, for each temperature, the densities in the liquid and vapor bulks. The predictions of the two different approaches compare well and this has provided a validation of the numerical code.

Afterward, the time evolution of the liquid bulk and interface region has been investigated based on the system of two coupled Enskog-Vlasov equations for the case of evaporation into near vacuum conditions. The simulated liquid temperatures have been in a range which gives rise to a sufficiently dilute vapor phase. Equilibrium solutions have been used as initial conditions and periodic boundary conditions have been replaced by moving absorbing surfaces. These surfaces have been placed sufficiently far away from the liquid-vapor interfaces so as not to perturbed them but, at the same time, close enough that collisions in the vapor phases can be disregarded.

The main results of this work are as follows:

(1) The equilibrium liquid-vapor coexistence diagrams have been mapped out for different compositions of the liquid phase.

(2) The distribution functions of the evaporated atoms have been determined. Previous findings relating to a single-component liquid have been confirmed. More specifically, at low temperatures the half-range Maxwellian with zero drift velocity and temperature equal to the liquid temperature provides a good approximation for the shape of the velocity distributions of emitted atoms. However, as the temperature increases, a better approximation is given by anisotropic Maxwellians with

different temperatures in the direction normal and parallel to the liquid-vapor interface. Furthermore, it has been found that these temperatures are closely related to the separation temperature, although a more detailed study is needed to fully support this conclusion.

(3) Evaporation coefficients have been computed. They turn out to be different for the two components and, in the simulation conditions, only mildly dependent on the liquid-vapor interface composition and temperature. Estimates of the evaporation coefficients have been obtained by evaluating the saturated vapor densities of the two components based on the maximum molar fraction of the less volatile component in the liquid phase and the separation temperature. This choice meets the need to possibly match the continuum description of the liquid phase and the kinetic description of the vapor phase.

The present study is only the first step toward a deeper understanding of evaporation processes that involve multicomponent liquids. Several research directions can be envisioned. These include a more detailed analysis of the distribution function anisotropy of evaporated atoms and the extension of the present results to mixtures of atoms having different diameters. This latter study would permit to treat the evaporation of the mixture of argon and krypton and to assess the predictions of the mean field kinetic theory approach with the MD results presented in Ref. [23]. The extension of Eqs. (6) and (7) to polydisperse mixtures is discussed in Ref. [57] while generalized expressions of the pair correlation functions, Eq. (5) and chemical potentials and pressure, Eqs. (10), can be obtained based on Ref. [42] and references therein. Additional interesting topics include the evaporation into a gas-vapor medium and the evaporation of micro-nano droplets. Indeed, the backscattered molecular flux from the vapor to the liquid and the surface tension due to the droplet curvature are anticipated to affect in a nontrivial way the evaporation process.

ACKNOWLEDGMENTS

This work has been financially supported in the UK by EPSRC Grants No. EP/N016602/1, No. EP/P020887/1, and No. EP/P031684/1) and the Leverhulme Trust.

[1] J. S. Rowlinson and B. Widom, *Molecular Theory of Capillarity* (Clarendon Press, Oxford, 1982).

[2] Y. Sone, Kinetic theoretical studies of the half-space problem of evaporation and condensation, Transport Theor. Stat. **29**, 227 (2000).

[3] T. Ytrehus, Molecular-flow effects in evaporation and condensation at interfaces, Mult. Scien. Techn. **9**, 205 (1997).

[4] T. Gombosi, A. Nagy, and T. Cravens, Dust and neutral gas modeling of the inner atmospheres of comets, Rev. Geophys. **24**, 667 (1986).

[5] C. J. Knight, Theoretical modeling of rapid surface vaporization with back pressure, AIAA J. **17**, 519 (1979).

[6] Y. Li and S.-L. Xu, DSMC simulation of vapor flow in molecular distillation, Vacuum **110**, 40 (2014).

[7] S. S. Sazhin, Modelling of fuel droplet heating and evaporation: Recent results and unsolved problems, Fuel **196**, 69 (2017).

[8] T. Ytrehus, Theory and experiments on gas kinetics in evaporation, Rarefied Gas Dynamics. Prog. Aeronaut. **51**, 1197 (1977).

[9] R. Ohse, J. Babelot, A. Frezzotti, K. Long, and J. Magill, Equation of state of uranium oxide: Mach-disk investigation of transient laser-induced vaporization of UO_2 up to 5000 K, High Temp.-High Press. **12**, 537 (1980).

[10] A. Frezzotti, Kinetic theory study of the strong evaporation of a binary mixture, in *Proceedings of the 15th International Symposium on Rarefied Gas Dynamics*, edited by V. Boffi, C. Cercignani (B. G. Teubner, Stuttgart, 1986), Vol. 2, p. 313.

[11] J. R. Ferron, Evaporation and condensation of mixtures under rarefied conditions, Ind. Eng. Chem. Fund. **25**, 594 (1986).
[12] S. Yasuda, S. Takata, and K. Aoki, Evaporation and condensation of a binary mixture of vapors on a plane condensed phase: Numerical analysis of the linearized Boltzmann equation, Phys. Fluids **17**, 047105 (2005).
[13] S. Takata and F. Golse, Half-space problem of the nonlinear Boltzmann equation for weak evaporation and condensation of a binary mixture of vapors, Eur. J. Mech. B **26**, 105 (2007).
[14] K. Aoki, S. Takata, and S. Kosuge, Vapor flows caused by evaporation and condensation on two parallel plane surfaces: Effect of the presence of a noncondensable gas, Phys. Fluids **10**, 1519 (1998).
[15] S. Kosuge, K. Aoki, and M. Hatano, Slow evaporation and condensation on a spherical droplet in the presence of a noncondensable gas, Phys. Fluids **22**, 067101 (2010).
[16] I. N. Shishkova, S. S. Sazhin, and J. Xie, A solution of the Boltzmann equation in the presence of inelastic collisions, J. Comput. Phys. **232**, 87 (2013).
[17] A. Frezzotti, G. P. Ghiroldi, L. Gibelli, and A. Bonucci, DSMC simulation of rarefied gas mixtures flows driven by arrays of absorbing plates, Vacuum **103**, 57 (2014).
[18] A. Frezzotti, Boundary conditions at the vapor-liquid interface, Phys. Fluids **23**, 030609 (2011).
[19] V. Zhakhovskii and S. Anisimov, Molecular-dynamics simulation of evaporation of a liquid, JETP **84**, 734 (1997).
[20] T. Ishiyama, T. Yano, and S. Fujikawa, Molecular dynamics study of kinetic boundary condition at an interface between argon vapor and its condensed phase, Phys. Fluids **16**, 2899 (2004).
[21] A. Lotfi, J. Vrabec, and J. Fischer, Evaporation from a free liquid surface, Int. J. Heat Mass **73**, 303 (2014).
[22] M. Heinen, J. Vrabec, and J. Fischer, Communication: Evaporation: Influence of heat transport in the liquid on the interface temperature and the particle flux, J. Chem. Phys. **145**, 081101 (2016).
[23] A. Frezzotti, Non-equilibrium structure of the vapor-liquid interface of a binary fluid, in *27th International Symposium on Rarefied Gas Dynamics*, AIP Conf. Proc. No. 1333 (AIP, New York, 2011), p. 161.
[24] K. Kobayashi, K. Sasaki, M. Kon, H. Fujii, and M. Watanabe, Kinetic boundary conditions for vapor-gas binary mixture, Microfluid. Nanofluid. **21**, 53 (2017).
[25] A. Frezzotti and P. Barbante, Kinetic theory aspects of non-equilibrium liquid-vapor flows, Mech. Eng. Rev. **4**, 16 (2017).
[26] C. Cercignani, *The Boltzmann Equation and Its Applications* (Springer, Berlin, 1988).
[27] C. Hahn, Z. R. Kann, J. A. Faust, J. Skinner, and G. M. Nathanson, Super-Maxwellian helium evaporation from pure and salty water, J. Chem. Phys. **144**, 044707 (2016).
[28] R. Marek and J. Straub, Analysis of the evaporation coefficient and the condensation coefficient of water, Int. J. Heat Mass **44**, 39 (2001).
[29] A. H. Persad and C. A. Ward, Expressions for the evaporation and condensation coefficients in the Hertz-Knudsen relation, Chem. Rev. **116**, 7727 (2016).
[30] R. Meland, A. Frezzotti, T. Ytrehus, and B. Hafskjold, Nonequilibrium molecular-dynamics simulation of net evaporation and net condensation, and evaluation of the gas-kinetic boundary condition at the interphase, Phys. Fluids **16**, 223 (2004).
[31] A. Frezzotti, L. Gibelli, and S. Lorenzani, Mean field kinetic theory description of evaporation of a fluid into vacuum, Phys. Fluids **17**, 012102 (2005).
[32] M. Kon, K. Kobayashi, and M. Watanabe, Method of determining kinetic boundary conditions in net evaporation/condensation, Phys. Fluids **26**, 072003 (2014).
[33] L. De Sobrino, On the kinetic theory of a van der Waals gas, Can. J. Phys. **45**, 363 (1967).
[34] M. Grmela, Kinetic equation approach to phase transitions, J. Stat. Phys. **3**, 347 (1971).
[35] J. Karkheck and G. Stell, Kinetic mean-field theories, J. Chem. Phys. **75**, 1475 (1981).
[36] A. Frezzotti and L. Gibelli, A kinetic model for equilibrium and non-equilibrium structure of the vapor-liquid interface, in *23rd International Symposium on Rarefied Gas Dynamics*, AIP Conf. Proc. No. 663 (AIP, New York, 2003), p. 980.
[37] A. Frezzotti, S. Nedea, A. Markvoort, P. Spijker, and L. Gibelli, Comparison of molecular dynamics and kinetic modeling of gas-surface interaction, in *26th International Symposium on Rarefied Gas Dynamics*, AIP Conf. Proc. Vol. 1084 (AIP, New York, 2008), p. 635.

[38] A. Frezzotti and L. Gibelli, A kinetic model for fluid-wall interaction, Proc. Inst. Mech. Eng., Part C **222**, 787 (2008).
[39] P. Barbante, A. Frezzotti, L. Gibelli, and D. Giordano, A kinetic model for collisional effects in dense adsorbed gas layers, in *27th International Symposium on Rarefied Gas Dynamics*, AIP Conf. Proc. No. 1333 (AIP, New York, 2011), p. 458.
[40] P. Barbante, A. Frezzotti, and L. Gibelli, A kinetic theory description of liquid menisci at the microscale, Kinet. Relat. Mod. **8**, 235 (2015).
[41] S. B. Yuste, A. Santos, and M. López de Haro, Structure of multi-component hard-sphere mixtures, J. Chem. Phys. **108**, 3683 (1998).
[42] A. Santos, S. B. Yuste, and M. L. De Haro, Equation of state of a multicomponent d-dimensional hard-sphere fluid, Mol. Phys. **96**, 1 (1999).
[43] N. F. Carnahan and K. E. Starling, Equation of state for nonattracting rigid spheres, J. Chem. Phys. **51**, 635 (1969).
[44] H. Van Beijeren and M. H. Ernst, The modified Enskog equation, Phys. (Amsterdam, Neth.) **68**, 437 (1973).
[45] J. Fischer and M. Methfessel, Born-Green-Yvon approach to the local densities of a fluid at interfaces, Phys. Rev. A **22**, 2836 (1980).
[46] H. T. Davis, Kinetic theory of inhomogeneous fluid: Tracer diffusion, J. Chem. Phys. **86**, 1474 (1987).
[47] A. Frezzotti, A particle scheme for the numerical solution of the Enskog equation, Phys. Fluids **9**, 1329 (1997).
[48] J. Hirschfelder, R. B. Bird, and C. F. Curtiss, *Molecular Theory of Gases and Liquids* (Wiley, New York, 1964).
[49] F. Kohler, J. Fischer, and E. Wilhelm, Intermolecular force parameters for unlike pairs, J. Mol. Struct. **84**, 245 (1982).
[50] S. Sumardiono and J. Fischer, Molecular dynamics simulations of mixture droplet evaporation, in *Eurotherm Seminar 77, Heat and Mass Transfer in Food Processing*, edited by J. Pagliarini and S. Rainieri, Vol. 77 (Edizione ETS Parma, Parma, 2005), p. 323.
[51] D. M. Heyes and A. Santos, Chemical potential of a test hard sphere of variable size in a hard-sphere fluid, J. Chem. Phys. **145**, 214504 (2016).
[52] J. Karkheck, E. Martina, and G. Stell, Kinetic variational theory for mixtures: Kac-tail limit, Phys. Rev. A **25**, 3328 (1982).
[53] M. P. Allen and D. J. Tildesley, *Computer Simulation of Liquids* (Oxford University Press, Oxford, UK, 1989).
[54] H. J. Berendsen, J. v. Postma, W. F. van Gunsteren, A. DiNola, and J. Haak, Molecular dynamics with coupling to an external bath, J. Chem. Phys. **81**, 3684 (1984).
[55] S. Cheng, J. B. Lechman, S. J. Plimpton, and G. S. Grest, Evaporation of Lennard-Jones fluids, J. Chem. Phys. **134**, 224704 (2011).
[56] P. Barbante and A. Frezzotti, A comparison of models for the evaporation of the Lennard-Jones fluid, Eur. J. Mech. B **64**, 69 (2017).
[57] M. Wendland, Born-Green-Yvon results for the liquid-vapour interface of pure fluids and binary model mixtures, Fluid Phase Equilib. **141**, 25 (1997).